Model Validation for Propulsion – On the TFNS and LES Subgrid Models for a Bluff Body Stabilized Flame

Thomas Wey[1]

NASA Glenn Research Center

Cleveland, Ohio 44135 USA

Abstract

This paper summarizes the reacting results of simulating a bluff body stabilized flame experiment of Volvo Validation Rig using a releasable edition of the National Combustion Code (NCC). The turbulence models selected to investigate the configuration are the subgrid scaled kinetic energy coupled large eddy simulation (K-LES) and the time-filtered Navier-Stokes (TFNS) simulation. The turbulence chemistry interaction used is linear eddy mixing (LEM).

Introduction

With advances in computational power and availability of distributed computers, the use of even the most complex of turbulent chemical interaction models in combustors and coupled analysis of combustors and turbines is now possible and more and more affordable for realistic geometries. It is well known that the major difficulty, when modeling the turbulence-chemistry interaction, lies in the high non-linearity of the reaction rate expressed in terms of the temperature and species mass fractions. The linear eddy model[1,2] (LEM), which uses local instantaneous values of the temperature and mass fractions, have been shown to often provide more accurate results of turbulent combustion. In the present, the time-filtered Navier-Stokes (TFNS) and K^{sgs}-LES approach capable of capturing unsteady flow structures important for turbulent mixing in the combustion chamber and a subgrid model, LEM-like capable of emulating the major processes occurring in the turbulence-chemistry interaction were used to perform reacting flow simulations of a MVP workshop selected test case. The selected test case from the Volvo Validation Rig was documented by Sjunnesson et al[3,4]**.**

The main purpose of this report is to compare the results, obtained from the TFNS approach and LES approach employing the LEM subgrid models, with the experimental data. The open source version (OpenNCC) of National Combustion Code (NCC) currently under-development at NASA Glenn Research Center is used for the calculations. It is a pre-conditioning enabled density based polyhedron finite–volume code which contains a wild range of numerical methods and models. It adopts the data structure of arbitrary polyhedrons that permit cells of arbitrary shape to be used: cells can have an arbitrary

[1] Research Aerospace Engineer, Engine Combustion Branch.

number of faces and faces can have an arbitrary number of points. A second order accurate central or upwind scheme is used for spatial discretization of the Euler fluxes in TFNS or LES governing equations. A third order accurate central scheme is available as well via Taylor series expansion for spatial discretization of the Euler fluxes. A second order accurate central scheme is used for discretization of the Laplacian terms in the governing equations. For the temporal integration, the options include: (1) non-iterative second order predictor-corrector MacCormack scheme; (2) dual-time sub-iterative 2-stage modified Maccormack scheme; (3) dual-time sub-iterative 3-4-5-stage Runge-Kutta scheme. Four available turbulence models in the code are summarized in Table 1 from the coding point of view.

Turbulence Model	Turbulence Stresses	Eddy Viscosity	K-Destruction Term	Coefficients
TFNS	Quadratic & Cubic	$C_\mu \rho K^2/\varepsilon$	$\rho\varepsilon$	RCP: Prescribed
K - LES	Linear	$C_\nu \rho K^{0.5}\Delta$	$C_\varepsilon \rho (K)^{1.5}/\Delta$	C_ν, C_ε: Prescribed or computed by LDKM scheme
LES	Linear	$(C_s\Delta)^2\rho\lvert S\rvert$	N/A	C_s, Prescribed
TFNS/LES	Quadratic & Cubic	$\mathrm{Min}(C_\mu \rho K^2/\varepsilon, (C_s\Delta)^2\rho\lvert S\rvert)$	$\mathrm{Max}(\rho\varepsilon, C_\varepsilon \rho (K)^{1.5}/\Delta)$	RCP: Prescribed C_ε, C_s: Prescribed

Table 1 Main Differences of Turbulence Models Seen From Coding

It also includes two sub-grid based turbulence chemistry interaction: Eulerian based probability density function (EUPDF) model and LEM model.

Results and Discussion

In the followings, one non-reacting case and one reacting case are performed. The combustor is a rectangular duct with a flame holder centered in the duct. The characteristic length of the triangular bluff body is 40 mm. A grid provided by MVP Workshop is downloaded. The grid has an approximate length-scale resolutions of 4 mm in flame regions. The 4-mm flame-region all-hexahedron grid consists of 809,080 elements (i.e. 800k grid) and 2,476,174 faces.

Non-Reacting Case:

In this case, the control volumes used are derived from the original 4mm grid via a polyhedral truncation technique[5] such that the revised grid is composed of 1,667,518 elements and 9,052,167 faces. Its face-to-element ratio is increased from 3.06 to 5.43 to achieve better flux exchange between elements for the mixing of the scalars. A represented plot of the grid is shown in Figure 1. A test run is conducted using the following boundary conditions. At the inlet, the mass flow rate is 0.2083 kg/s, the static temperature is 288.2 K. The back pressure is set to 100,000 Pa. All walls are no-slip and adiabatic. From Figures 2 to 5, the contours of the instantaneous x-velocity, y-velocity,

pressure and z-vorticity are shown respectively. It is observed that the vortex shedding is very noticeable due to higher face to element ratio in the grid.

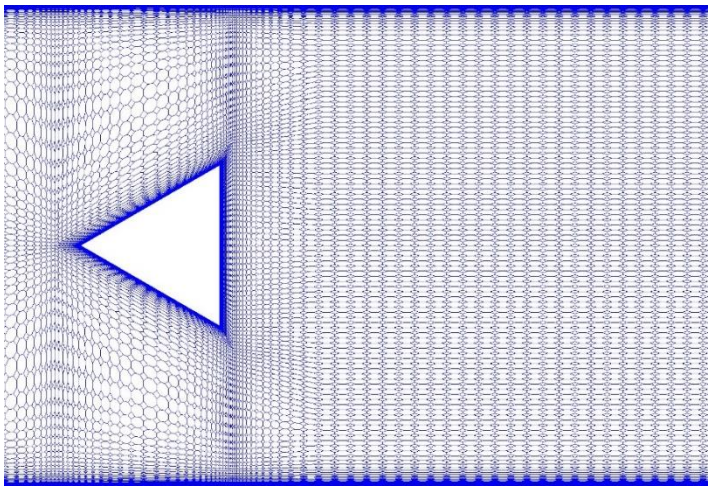

Figure 1 A middle plane cut of the grid. Number of elements is 1,667,518. Number of faces is 9,052,167. Face to element ratio is 5.43.

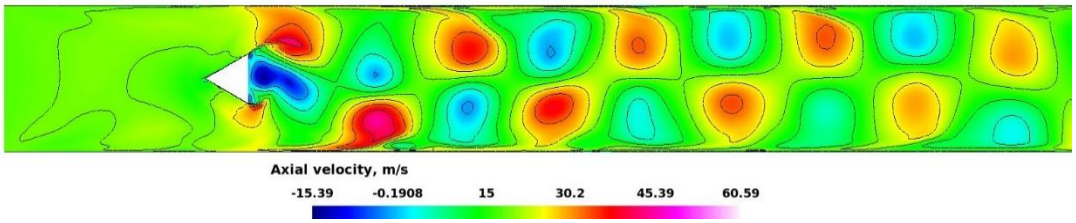

Figure 2 Instantaneous axial velocity contours for the non-reacting case.

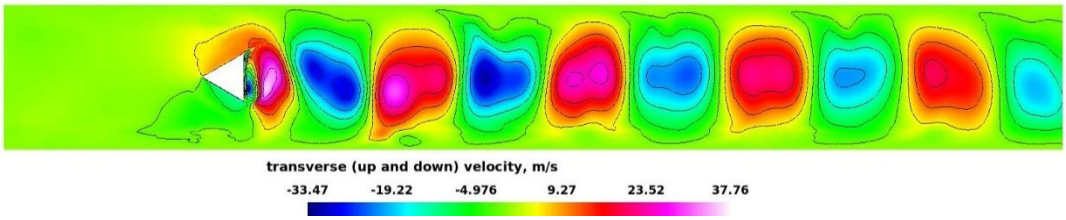

Figure 3 Instantaneous Y-velocity contours for the non-reacting case.

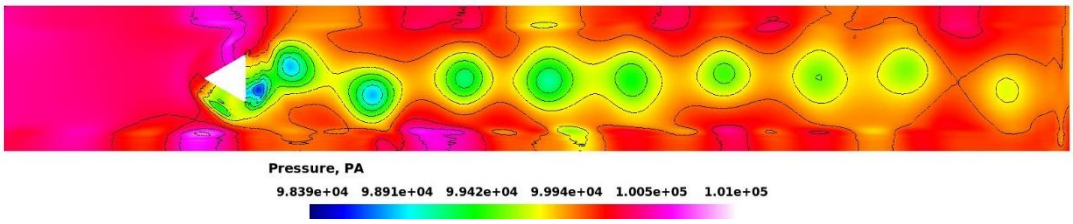

Figure 4 Instantaneous pressure contours at mid-plane of the domain for the non-reacting case.

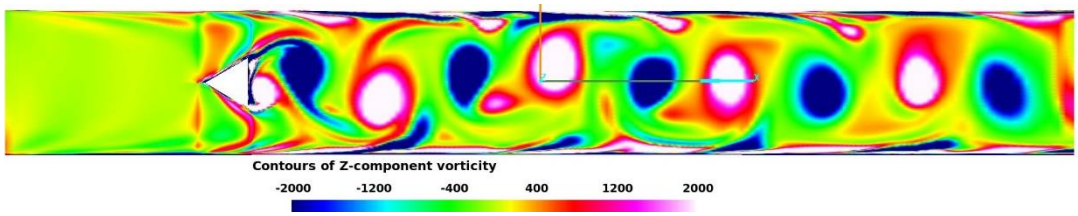

Figure 5 Instantaneous Z-vorticity contours at mid-plane for the non-reacting case.

From Figures 6 to 7, the contours of the averaged x-velocity and pressure are shown respectively.

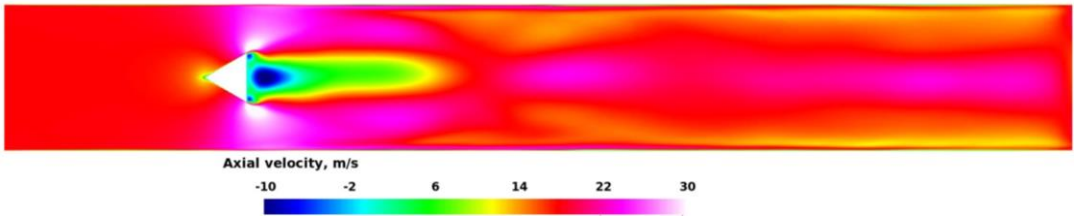

Figure 6 Averaged axial velocity contours for the non-reacting case.

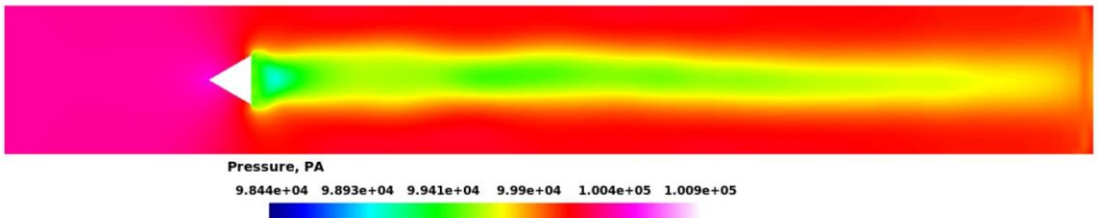

Figure 7 Averaged pressure contours for the non-reacting case.

Reacting case :

In this case, the original 800k grid download from the workshop webpage is used as shown in Figure 8.

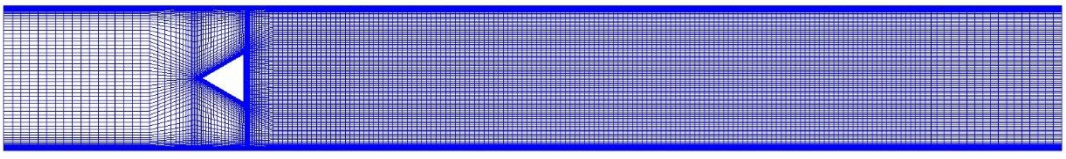

Figure 8 Computational grid (provided by workshop): Number of elements is 809,080. Number of faces is 2,476,174. Face to element ratio is 3.06.

The boundary conditions are set as follows: At the inlet, the mass flow rate is 0.2083 kg/s, the bulk inlet velocity is 17.3 m/s, the static temperature is 288.2 K, the mass fraction of C3H8 is 0.04 whose equivalence ratio is 0.65. The pressure of the exhaust gas is set to a constant of 100,000 Pa. All the walls are non-slip and adiabatic. The liner gradient is used for the momentum and enthalpy on the boundary. For other variables, zero gradient is used on the boundary. The variables on the periodic patch along the

z-axis are interpolated linearly.

For the finite-rate chemistry, instead of using the recommended mechanism from the workshop webpage, a global two-step chemical kinetic mechanism is used as below:

REACTIONS					cgs	Cal/mol
2 C3H8	+ 7 O2	= >	6 CO	+8 H2O	1.0E+12	33000
GLO / C3H8	0.9028/					
GLO / O2	0.6855/					
2 CO	+ 1 O2	< = >	2 CO2		2.25E+10	12000
GLO / CO	1.0/					
GLO /O2	0.5/					

This set of mechanism is quite similar to the one recommended by the workshop. The changes are: (1) The stoichiometric coefficients of the reaction kinetics have been multiplied by 2 to be became integers because the code accepts integer stoichiometric coefficients only and thus the pre-exponential factor of reaction constants have been divided by 2. (2) The global modifiers have been applied to the second kinetics as well for a stable reaction simulation. The turbulent combustion closure models, LEM-like model and well-defined model (i.e. laminar-chemistry), were used to perform reacting flow simulations.

To assess the influences of the turbulence models for the current case, two models were selected for simulations, one is the time-filtered Navier-Stokes (denoted TFNS) approach, the other is the sub-grid kinetic energy based LES approach, denoted K-LES. The resolution control parameter (RCP) in TFNS is set to 0.5 for the 800k grid. The coefficient, C_ν, of K-LES eddy viscosity is 0.067 initially and the coefficient, C_ε, of the destruction term of kinetic energy transport equation is 0.916 initially. The option to compute them (C_ν and C_ε) using the "localized dynamic kinetic energy model" (LDKM) is turned on later.

The results of three simulations on the 800k grid are presented in this case: (1) K-LES turbulence model with laminar chemistry, (2) K-LES with LEM as turbulence chemistry interaction (denoted K-LES-LEM), (3) TFNS turbulence model with laminar chemistry. The size of the time step is set to 5.E-7 second for all the simulations. The numerical algorithm is based upon a two-stage modified MacCormack predictor-corrector scheme such that the dual time stepping numerical convergence acceleration technique is achieved.

From Figures 9 to 12, the mid-plane contours of the instantaneous axial-velocity, Y-velocity, pressure and temperature are shown for three simulations, K-LES, K-LES-LEM and TFNS respectively. It is observed that the sizes of the recirculation zones for the reacting cases are larger than that of non-reacting case. The sizes of the recirculation zones among three reacting simulations are similar. The patterns of the pressure are quite similar among the three simulations. The similarity of the temperature patterns is also noticeable.

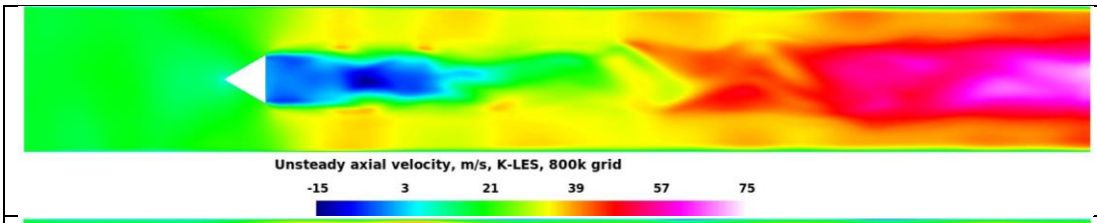

K-LES

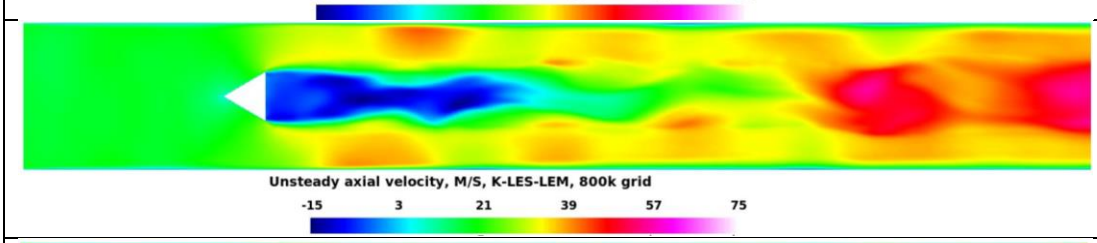

K-LES-LEM

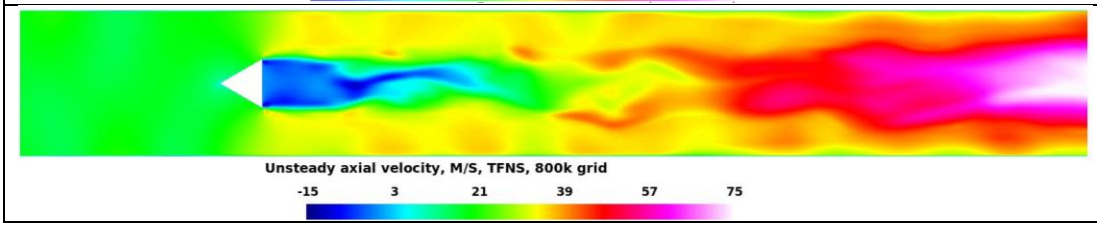

TFNS

Figure 9 Instantaneous axial velocity (M/S) contours of a two-step global kinetic reaction model for propane

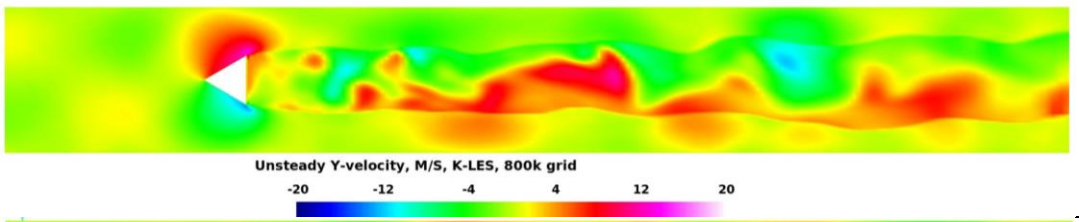

K-LES

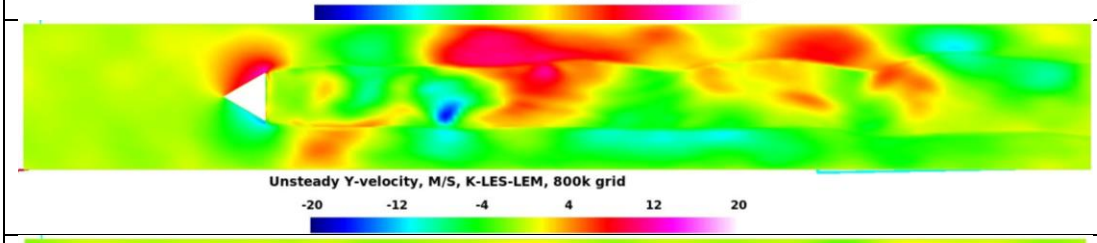

K-LES-LEM

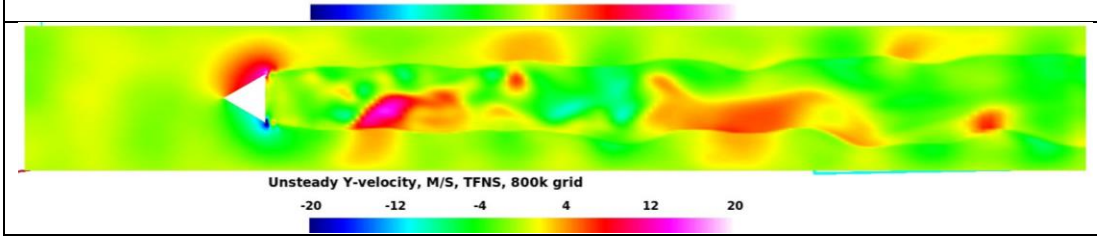

TFNS

Figure 10 Instantaneous Y-velocity (M/S) contours of a two-step global kinetic reaction model for propane

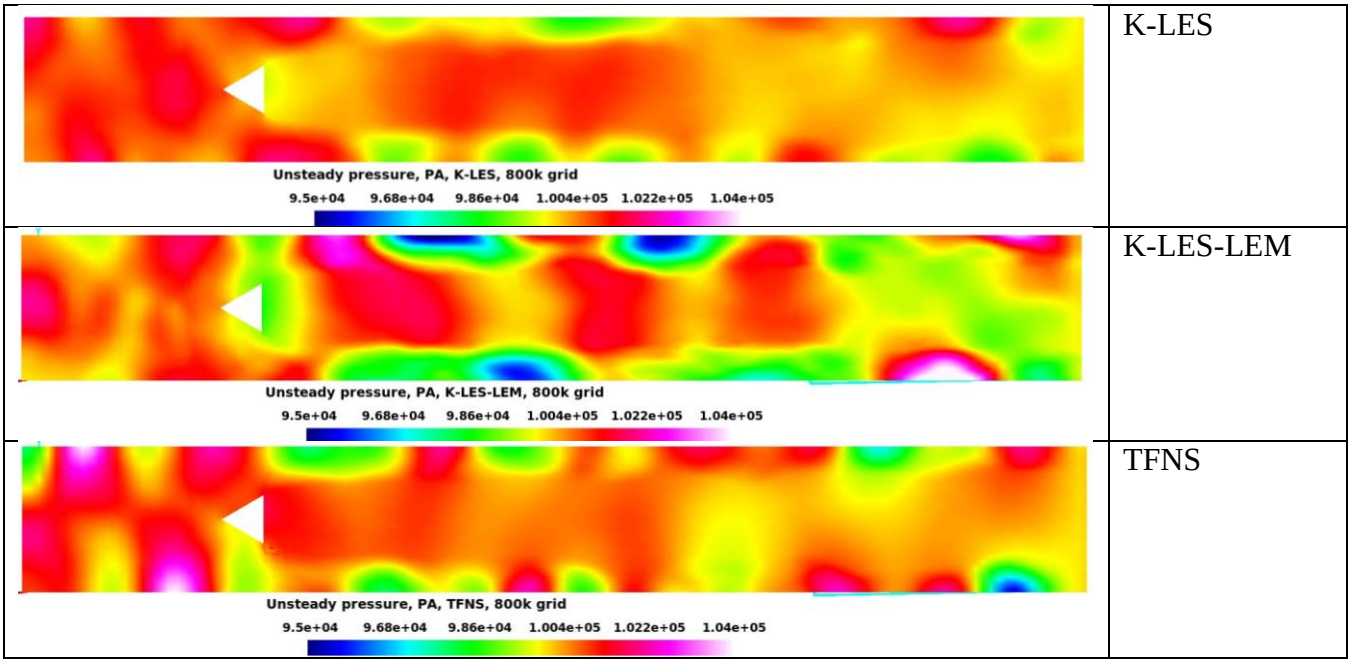

Figure 11 Instantaneous static pressure (PA) contours of a two-step global kinetic reaction model for propane

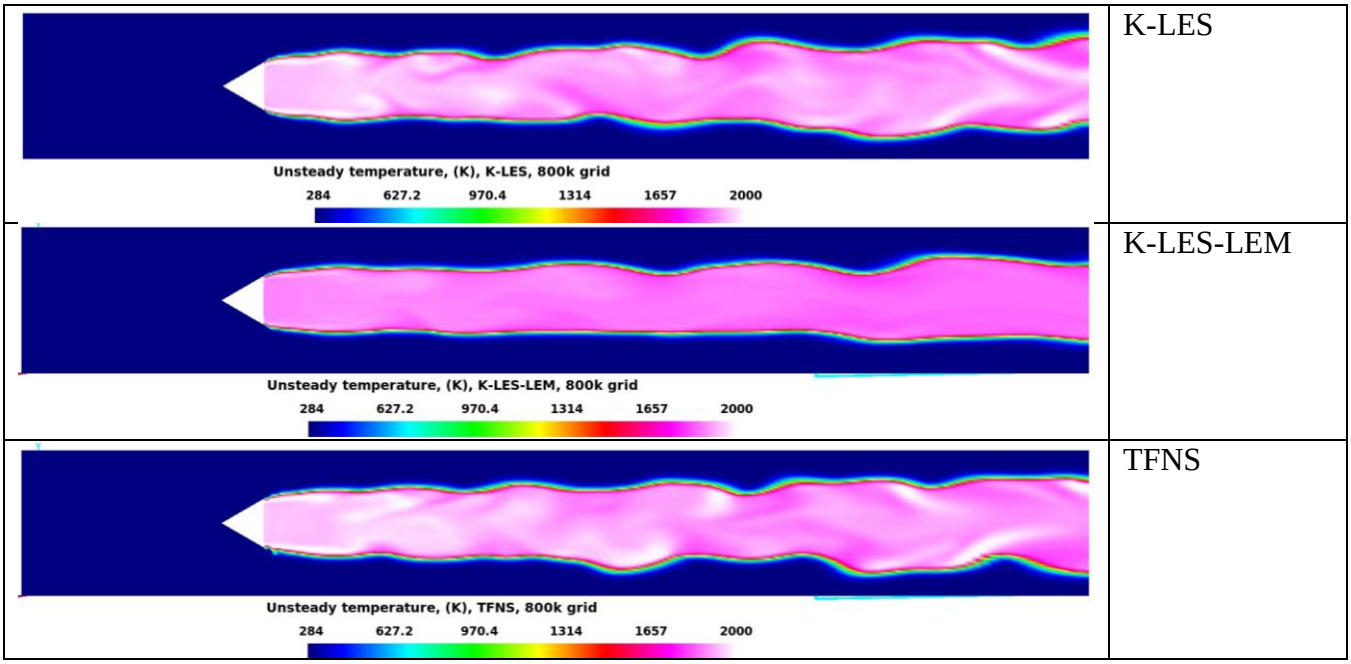

Figure 12 Instantaneous temperature (K) contours of a two-step global kinetic reaction model for propane

The mean values of all variables are computed at the end of the simulations by ensembling each time-step values of varibles inside the code. However, all the root mean square values of fluctuation of variables in the current work are postprocessed from limited sets of unsteady data due to the limits of the available disk spaces. Time averaged results from all three simulations are shown after Figure 13. All velocities and their fluctuations are normalied by the bulk inlet velocity, 17.3 m/s. All coordinates are normalized by the bluff body size, 0.04 m.

Figure 13 depicts the normalized mean axial volocity profiles of all three simulations along the combustor center line, behind the bluff body. The numerical results match the experimental data in general. The results of K-LES and K-LES-LEM are closer to experimental data than that of TFNS. Centerline profiles for the normalized fluctuation level on the 800k grid for reacting solutions are shown in Figure 14. Due to the number of unsteady data sets being saved is quite limited, the comparisons to the experimental data for all three simulations are poor except portion of K-LES profile.

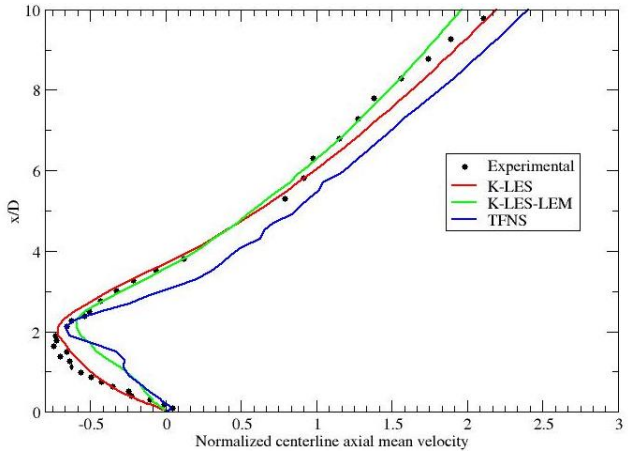

Figure 13 Centerline profiles for the normalized mean axial velocity on the 800k grid for reacting solutions from K-LES, K-LES-LEM and TFNS options.

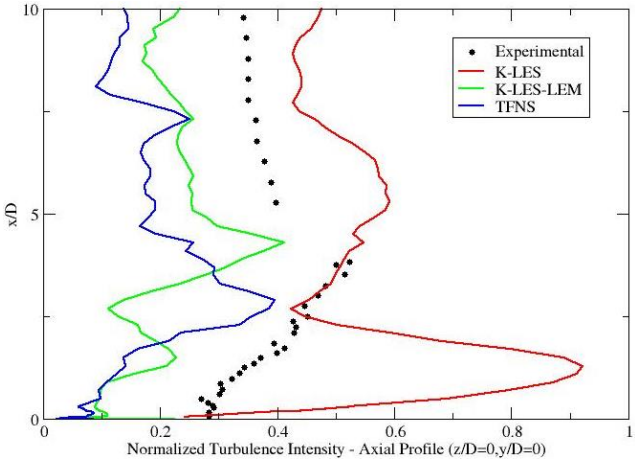

Figure 14 Centerline profiles for the normalized fluctuation level on the 800k grid for reacting solutions. However, all the root mean square values of fluctuation of variables in the current work are computed from limited sets of unsteady data due to the limits of the available disk spaces.

In the transverse direction, the normalized mean axial velocities of three simulations at the different axial locations are seen in Figure 15, from **a** to **g**. The accuracy of the numerical results is acceptable compared to the experimental data. The results of K-LES and K-LES-LEM are closer to experimental

data than that of TFNS in these figures overall.

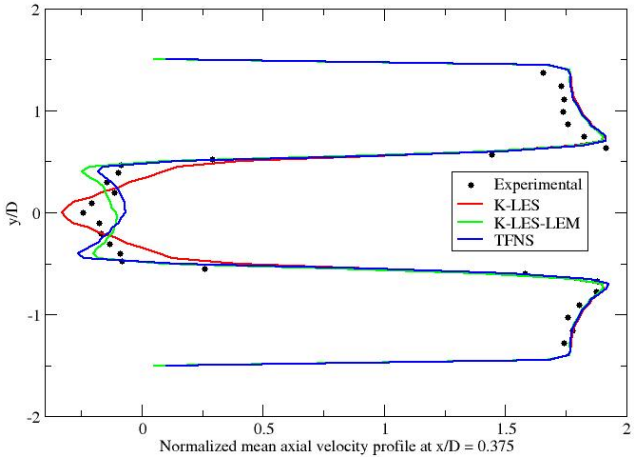

a. x/D = 0.375

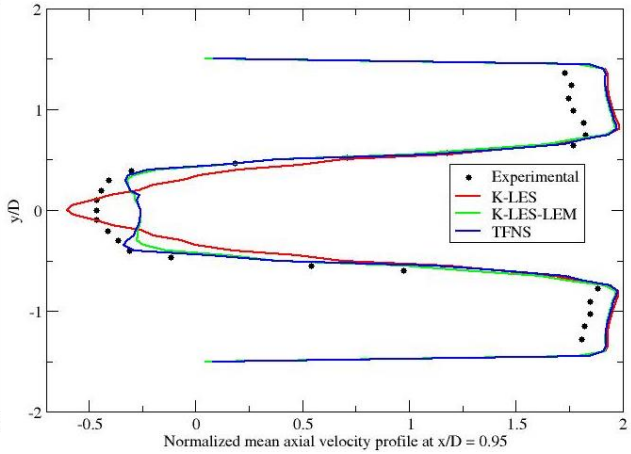

b. x/D = 0.95

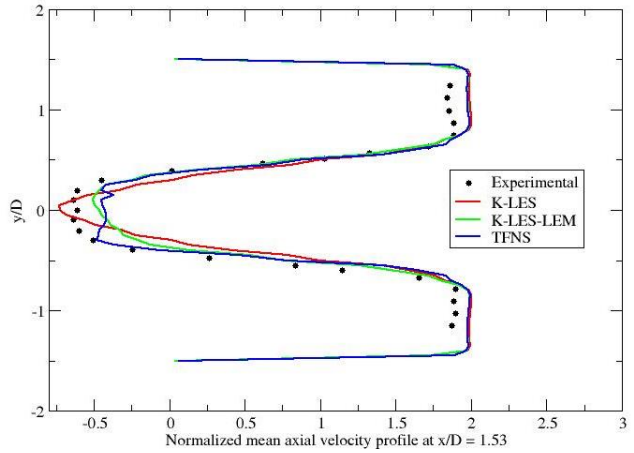

c. x/D = 1.53

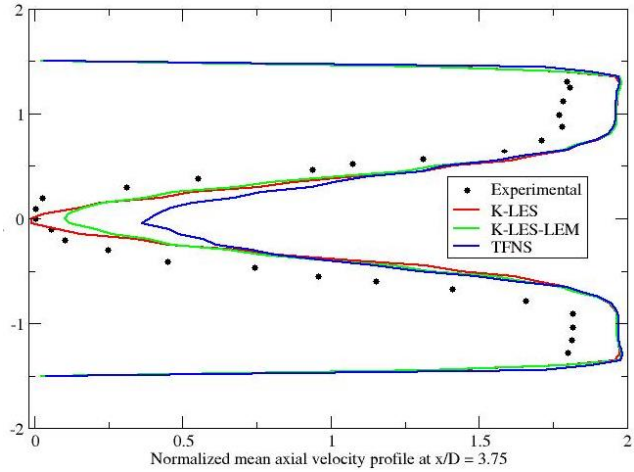

d. x/D = 3.75

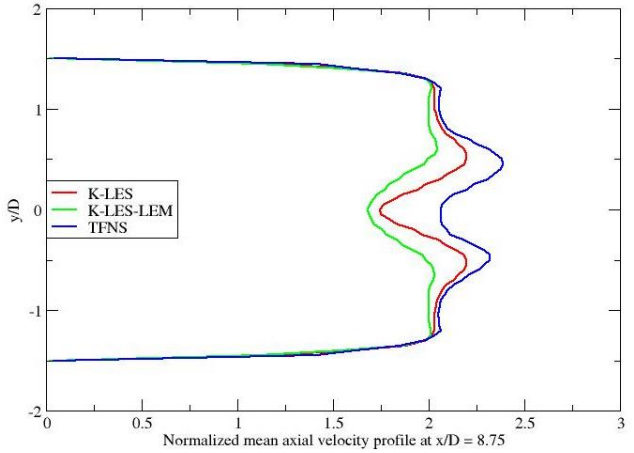

e. x/D = 8.75

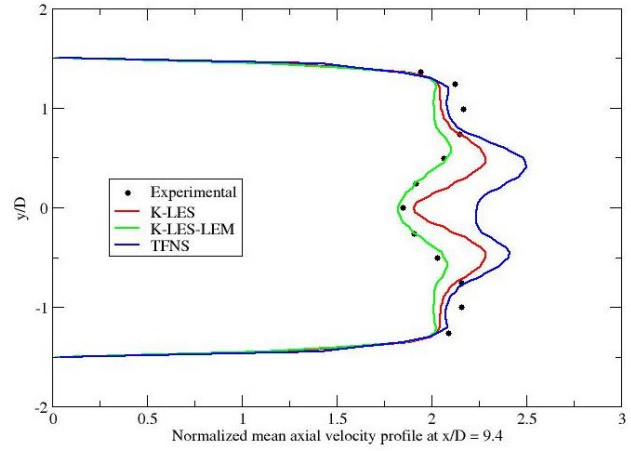

f. x/D = 9.4

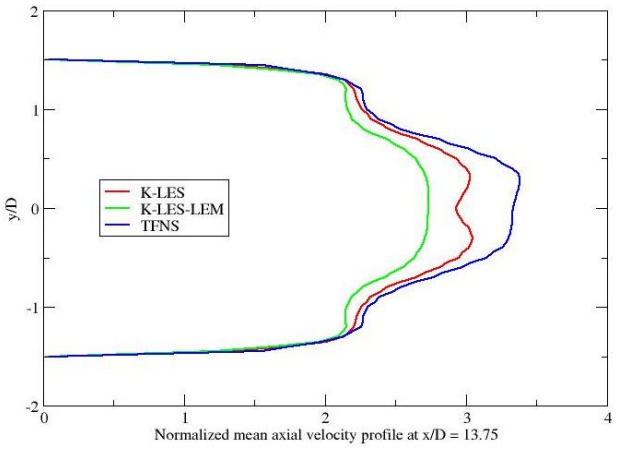

g. x/D = 13.75

Figure 15 Transverse profiles of normalized mean axial velocity at different axial locations.

The transverse profiles for the normalized fluctuation level of the axial velocity at the different axial locations are shown in Figure 16, from **a** to **g**. The comparisons to the experimental data for all three simulations are poor in general. In Figures 16.a, 16.b and 16.c, the accuracy of some portion of K-LES profile is acceptable.

In Figures 16.a, 16.b and 16.f, the accuracy of some portion of K-LES-LEM profile is acceptable. The results of K-LES and K-LES-LEM are closer to experimental data than that of TFNS in these figures overall. The experimental data is enclosed by the combined numerical data.

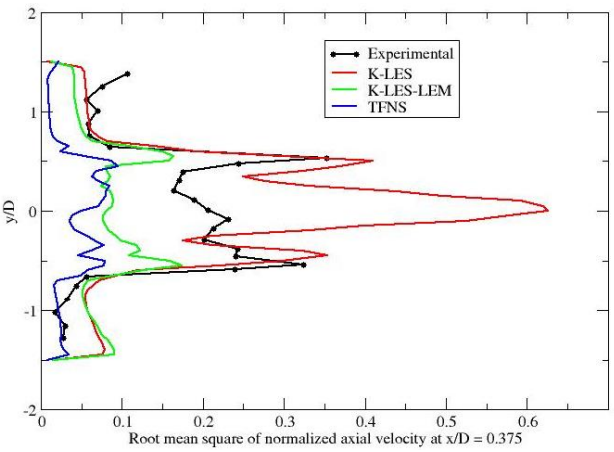

a. x/D = 0.375

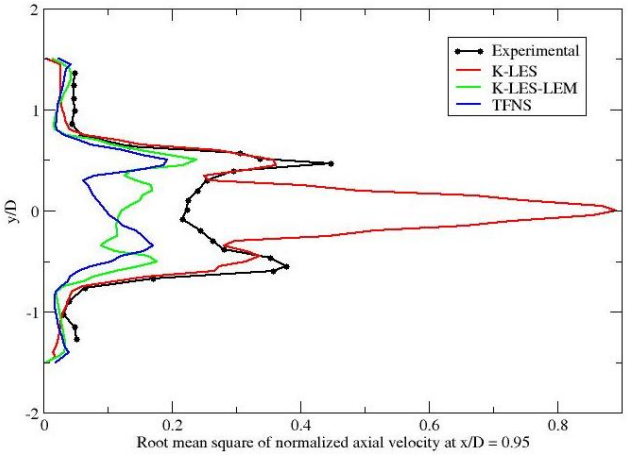

b. x/D = 0.95

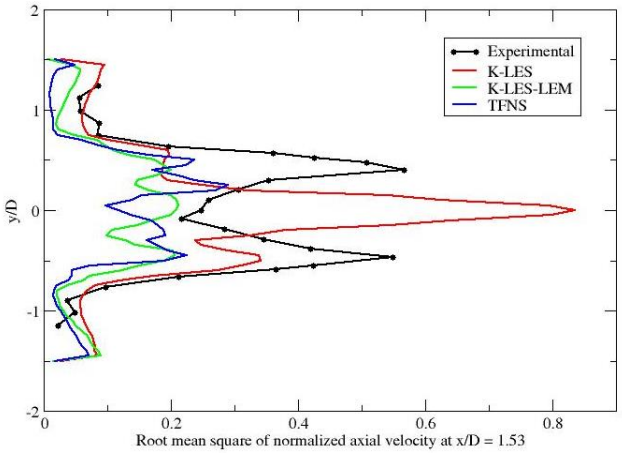

c. x/D = 1.53

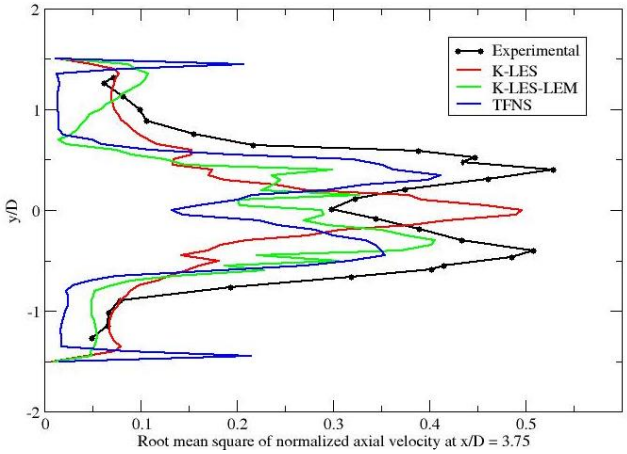

d. x/D = 3.785

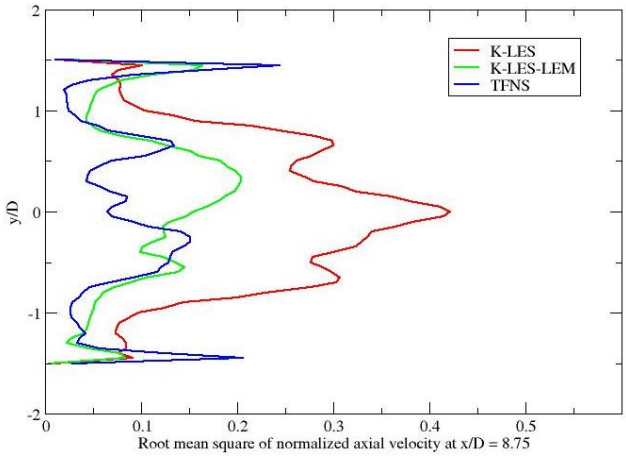

e. x/D = 8.75

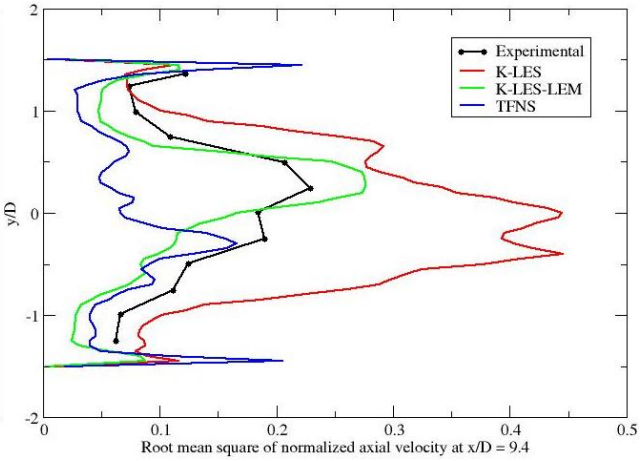

f. x/D = 9.4

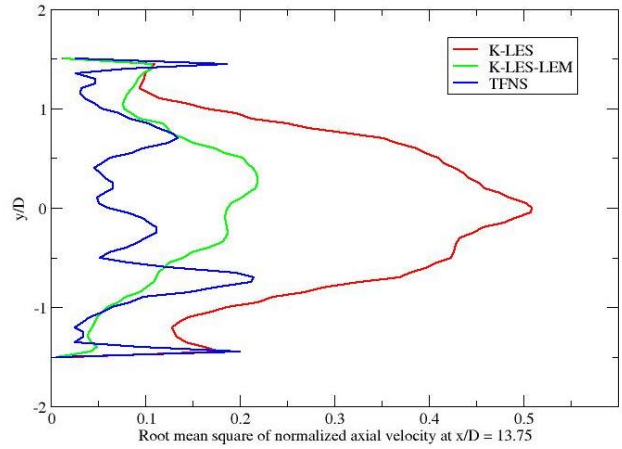

g. x/D = 13.75

Figure 16 Transverse profiles of normalized axial RMS velocity at different axial locations.

In the transverse direction, the normalized mean Y-velocities of three simulations at the different axial locations are seen in Figure 17, from **a** to **g**. The accuracy of the numerical results is acceptable

compared to the experimental data. The results of K-LES and K-LES-LEM are closer to experimental data than that of TFNS in these figures overall.

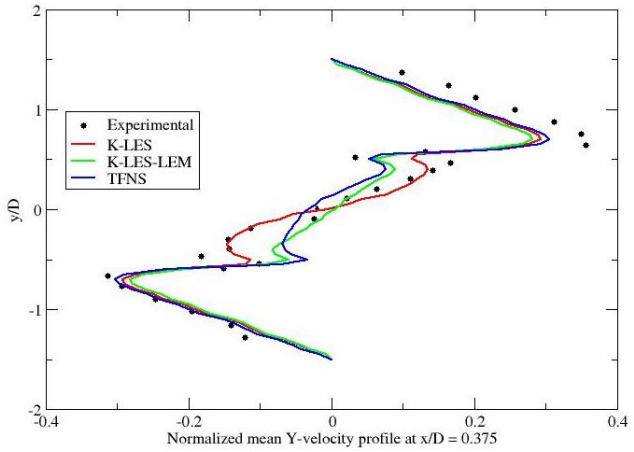

a. x/D = 0.375

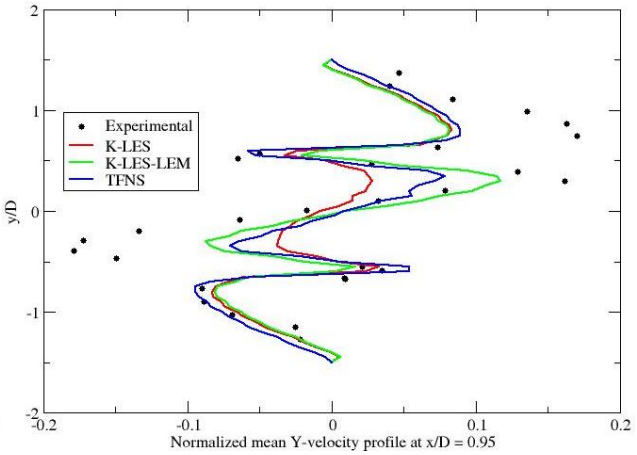

b. x/D = 0.957

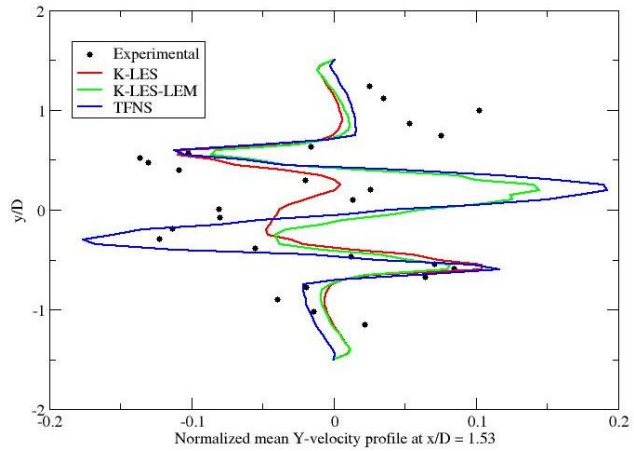

c. x/D = 1.54

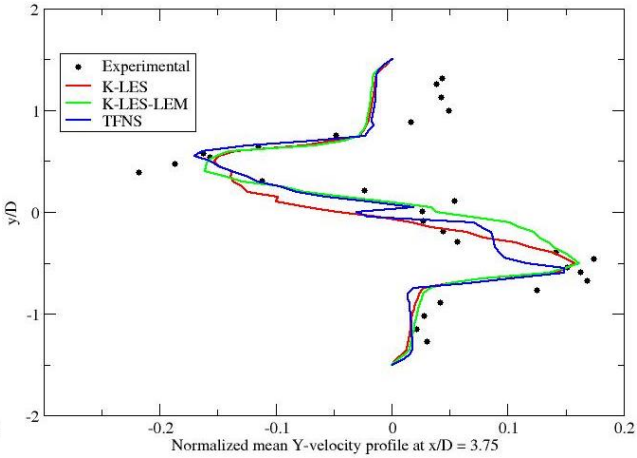

d. x/D = 3.75

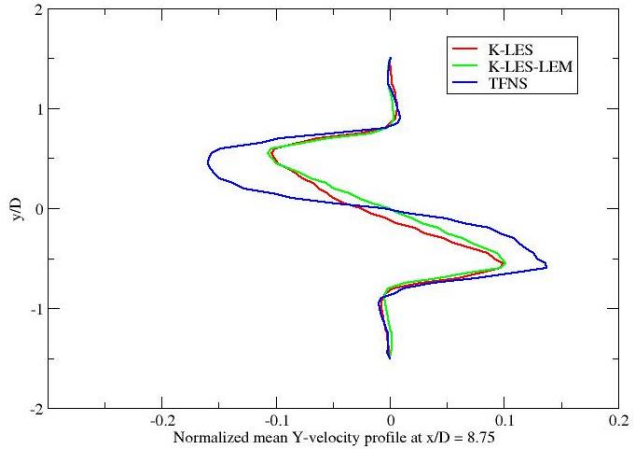

e. x/D = 8.75

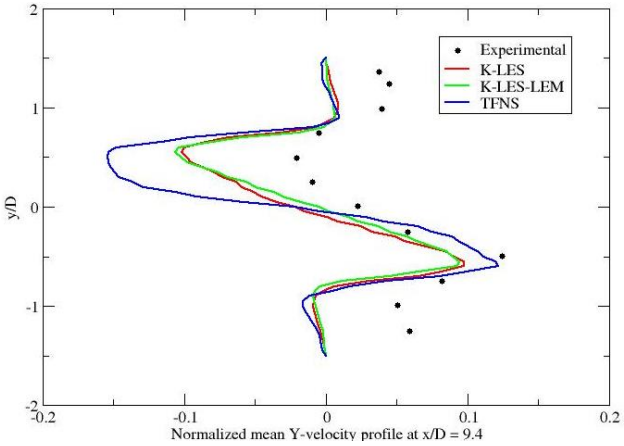

f. x/D = 9.4

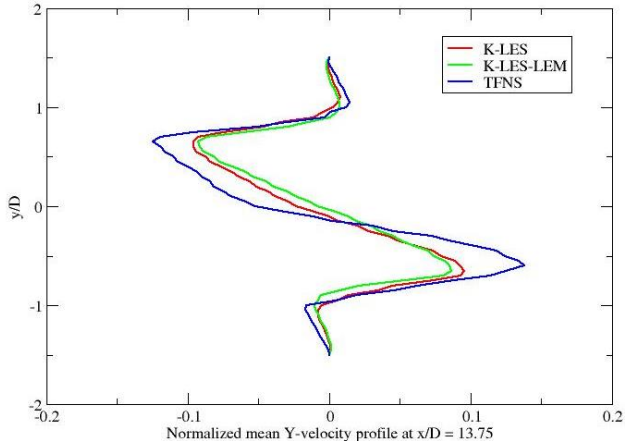

g. x/D = 13.75

Figure 17 Transverse profiles of normalized mean Y-velocity at different axial locations.

The transverse profiles for the normalized fluctuation level of the Y-velocity at the different axial locations are shown in Figure 18, from **a** to **g**. The comparisons to the experimental data for all three simulations are poor in general. In Figures 18.a, the accuracy of some portion of K-LES profile is acceptable. In Figures 18.b, the accuracy of some portion of K-LES-LEM profile is acceptable. In Figures 18.b, the accuracy of some portion of TFNS profile is acceptable.

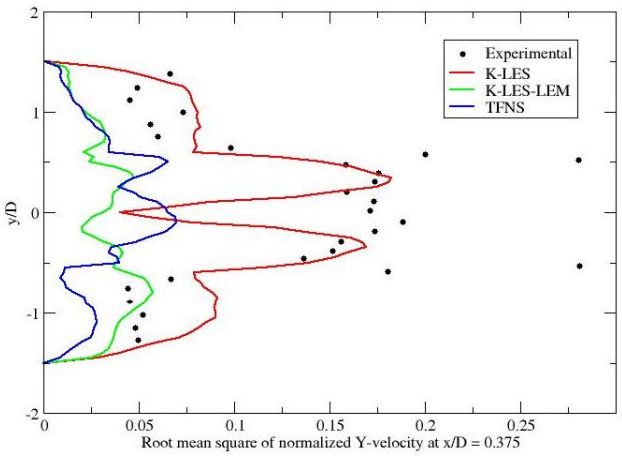

a. x/D = 0.375

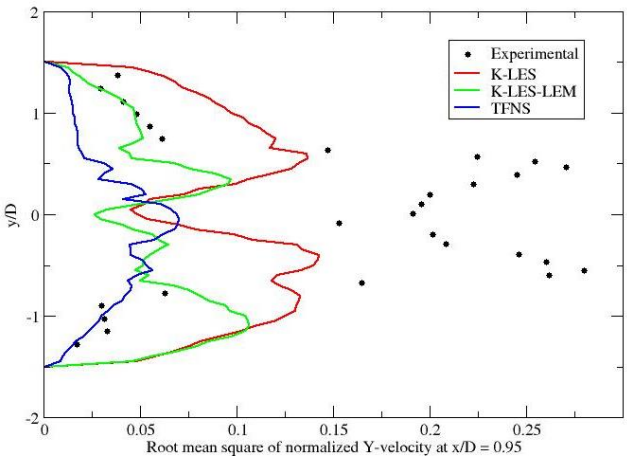

b. x/d = 0.95

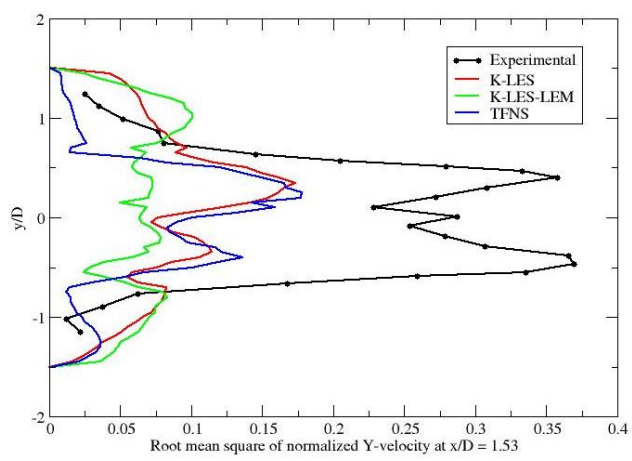

c. x/D = 1.53

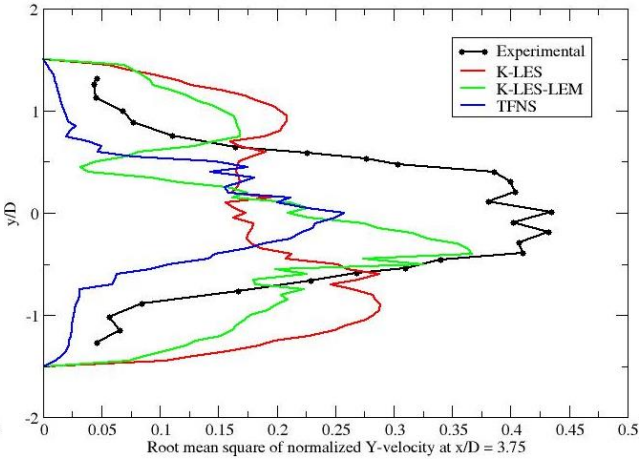

d. x/d = 3.75

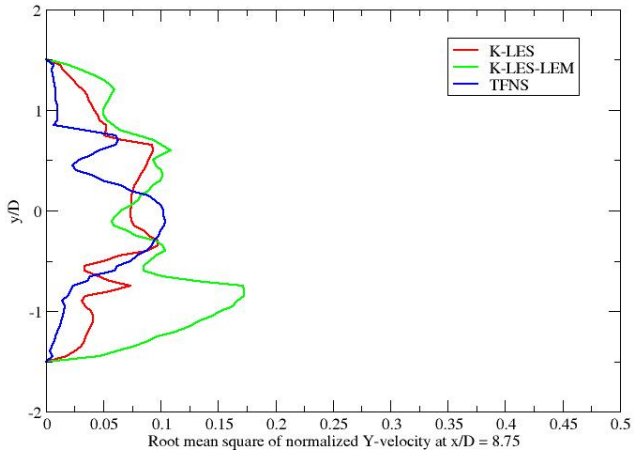

e. x/D = 8.75

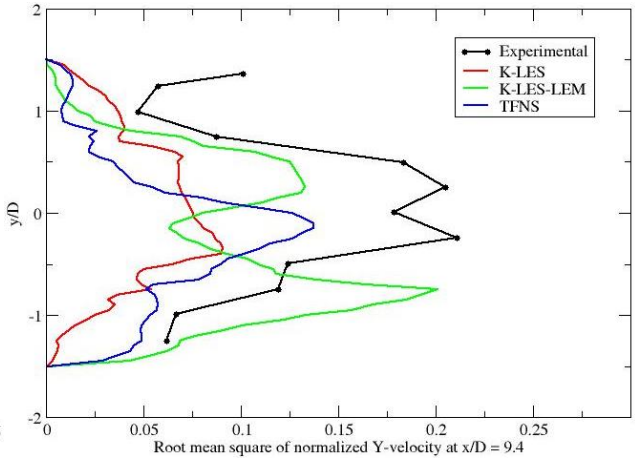

f. x/D = 9.4

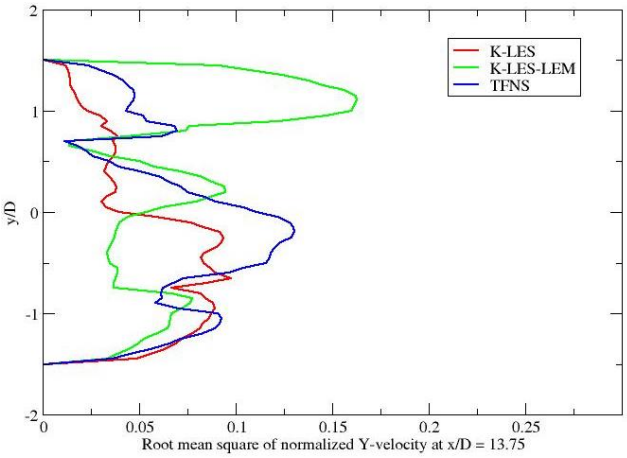

g. x/D = 13.75

Figure 18 Transverse profiles of normalized RMS Y-velocity at different axial locations.

In the transverse direction, the mean temperature of three simulations at the different axial locations are seen in Figure 19, from **a** to **g**. The accuracy of the numerical results is poor compared to the

experimental data. The overpreditons of the temperature by all three simulations are that understandably because the global kinetic mechanism is used. The results of K-LES and K-LES-LEM are closer to experimental data than that of TFNS in these figures overall.

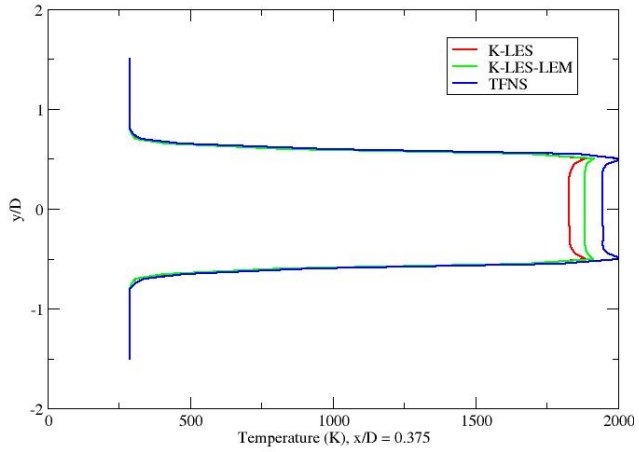

a. x/D = 0.375

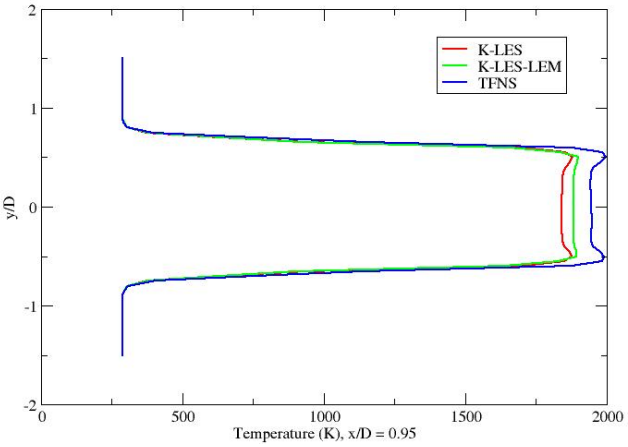

b. x/D = 0.95

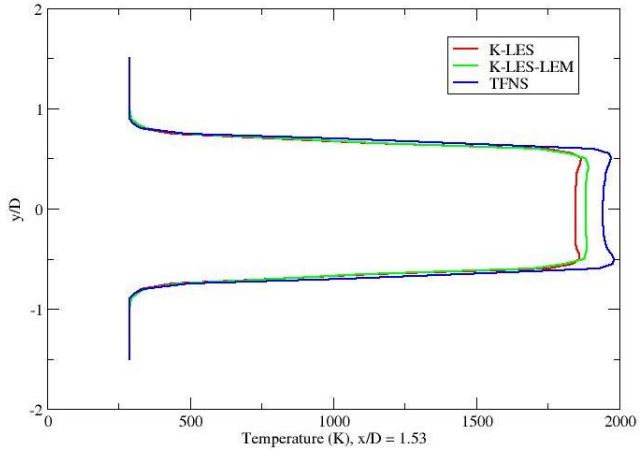

c. x/D = 1.53

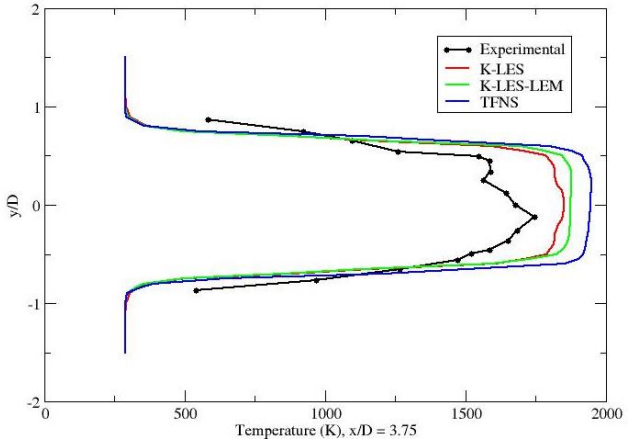

d. x/D = 3.75

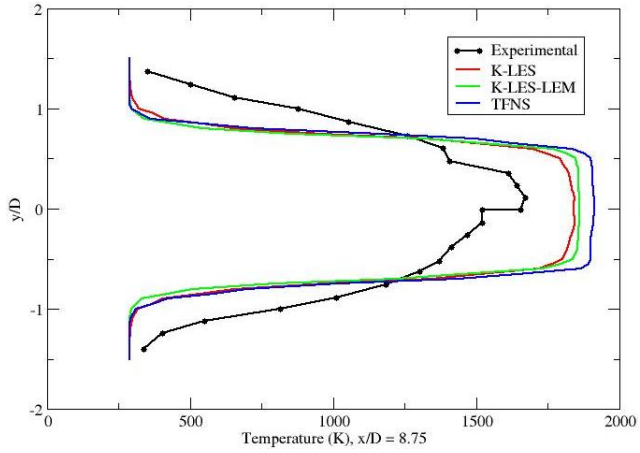

e. x/D = 8.75

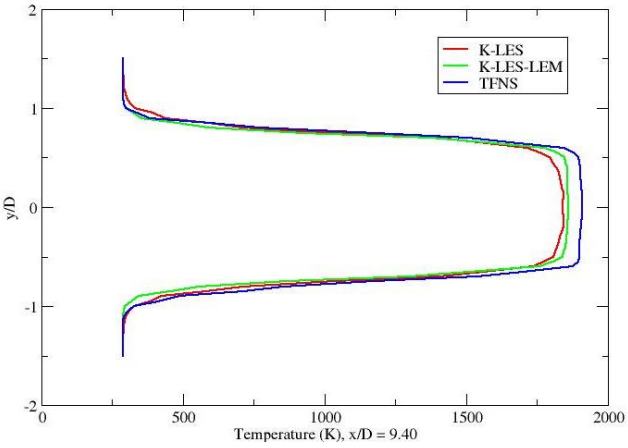

f. x/D = 9.4

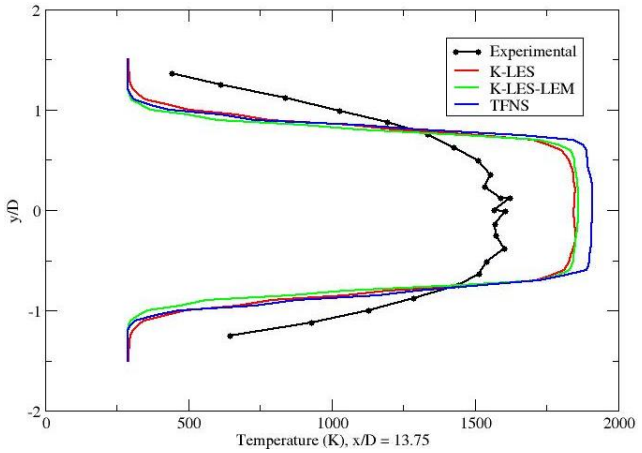

g. x/D = 13.75

Figure 19 Transverse profiles of mean temperature (K) at different axial locations.

Concluding Remarks

In the present work a bluff-body flame holder configuration is investigated with K-LES, K-LES-LEM and TFNS approaches on a 800k grid downloaded from the workshop webpage. All three reacting simulations predict that the flame is symmetric. All three reacting simulations produce time averaged axial velocities that are comparable to the experimental data in the recirculation zone. The time averaged Y-velocities are predicted less accurately compared to the experimental data in the recirculation zone. All three reacting simulations over-predict the mean temperature due to global mechanism. All reacting turbulence fluctuations are poorly predicted due to not sufficient unsteady data saved. Finally, for the current work, the most important factor that determines the quality of the reacting simulations is the lack of the proper reaction kinetics.

Acknowledgements

This work was supported by the NASA Transformational Tools and Technologies (TTT) project under the Transformative Aeronautics Concepts (TACP) program.

References

[1]Wey, T. C. and Liu, N.-S., "Assessment of Turbulence-Chemistry Interaction Models in the National Combustion Code (NCC) –Part I," AIAA 2010-1170, 48th AIAA ASM, Jan. 4-7, 2010, Orlando, FL.

[2]Menon, S., Sankaran, V., and Stone, C., "Subgrid Combustion Modeling for the Next Generation National Combustion Code," NASA CR 2003-212202

[3]Sjunnesson, A., Olovsson, S. and Sjoblom, B., "Validation Rig –A Tool for Flame Studies," International Society for Air-breathing Engines Conference, ISABE-91-7038, Nottingham, United Kingdom, 1991.

[4]Sjunnesson, A. Nelsson, C. and Max, E., "LDA Measurements of Velocities and Turbulence in a Bluff Body Stabilized Flame", Forth International Conference on Laser Anemometry-Advances and

Application, ASME, Cleveland, OH, 1991

[5]Wey, T. C. and Liu, N.-S., "Simulation of a Single-Element Lean-Direct Injection Combustor Using Arbitrary Polyhedral Mesh," AIAA 2012-0204, 50th AIAA ASM, Jan. 9-12, 2012, Nashville, TN.